

Temporal Convolutional Network Based Signal Detection for Magnetotactic Bacteria Communication System

Chenyao Bai*, Member, IEEE, Aoji Zhu*, Student Member, IEEE, Xiwen Lu, Student Member, IEEE, Yunlong Zhu, Kezhi Wang, Member, IEEE

Abstract—Molecular communication (MC) aims to use signaling molecules as information carriers to achieve communication between biological entities. However, MC systems severely suffer from inter symbol interference (ISI) and external noise, making it virtually difficult to obtain accurate mathematical models. Specifically, the mathematically intractable channel state information (CSI) of MC motivates the deep learning (DL) based signal detection methods. In this paper, a modified temporal convolutional network (TCN) is proposed for signal detection for a special MC communication system which uses magnetotactic bacteria (MTB) as information carriers. Results show that the TCN-based detector demonstrates the best overall performance. In particular, it achieves better bit error rate (BER) performance than sub-optimal maximum a posteriori (MAP) and deep neural network (DNN) based detectors. However, it behaves similarly to the bidirectional long short term memory (BiLSTM) based detector that has been previously proposed and performs worse than the optimal MAP detector. When both BER performance and computational complexity are taken into account, the proposed TCN-based detector outperforms BiLSTM-based detectors. Furthermore, in terms of robustness evaluation, the proposed TCN-based detector outperforms all other DL-based detectors.

Index Terms—Deep Learning, Magnetotactic Bacteria, Molecular Communication, Quorum Sensing, Signal Detection, Temporal Convolutional Network.

I. INTRODUCTION

In contrast to conventional communication systems, molecular communication (MC) encodes information into specific characteristics of signaling molecules, such as number, type, and time of release [1], which is a promising candidate for reliable communication between nanomachines. In MC, the transmitter releases the signaling molecules, which would then propagate in the medium and some of the molecules may arrive

at the receiver. Due to the advantages in terms of biocompatibility, minimal invasiveness and energy efficiency, MC has potential applications in multiple areas such as biomedical field (e.g., targeted drug delivery and tissue regeneration), environmental area (e.g., quality control), military applications (e.g., multifunctional equipment), and can be considered as an effective complement of the EM-based communications [2].

For both mathematical modeling and experimental deployment of MC systems, the reliable recovery of transmitted signals at the receiver is crucial. In particular, the information symbols or sequences are required to be detected after transmitting over a noisy and corrupted channel through specific detection schemes [1]. Due to the effect of inter symbol interference (ISI), the sequence-to-sequence detector outperforms the symbol-by-symbol counterparts as the information of previously transmitted symbols are considered. In general, the instantaneous or statistical channel state information (CSI) [3] is required for MC detectors, e.g., maximum likelihood (ML) detector and Maximum A Posteriori (MAP) detector [4]. The CSI can be theoretically obtained only within some specific conditions with the known system parameters. However, for practical implementations, due to the environmental complexity of MC, existing research is mostly based on plenty of assumptions, making it extremely challenging to establish precise models. Also, since MC system is susceptible to external interference, the derivation and estimation of CSI is complicated, which leads to difficulties in validating the theoretical models through experiments and a decline in detection performance.

The above-mentioned problems motivate the utilization of deep learning (DL) techniques to deal with signal detection, as well as other tasks for MC systems [5]–[7]. DL-based approaches use dataset containing samples of transmitted and received signal to train a detector and eventually achieve information recovery without analyzing the underlying channel model. Compared with other machine learning methods, DL has stronger robustness to noise, and has associative memory function, which can fully approximate complex nonlinear relationships [8].

The first important difference between our work and prior works is the underlying mathematical model of MC. Most existing studies focus on diffusion-based MC (DMC) models [9]–[11]. In recent years, fluid drift based MC has also been

This work was supported by China Postdoctoral Science Foundation (Grant No. 2021M690701). (Corresponding author: Yunlong Zhu)

Chenyao Bai, Aoji Zhu, Xiwen Lu and Yunlong Zhu are with the Academy for Engineering and Technology, Fudan University, Shanghai 200433, China. (e-mail: baichenyao@fudan.edu.cn; ajzhu21@m.fudan.edu.cn; xwlu21@m.fudan.edu.cn; zyl@fudan.edu.cn).

Kezhi Wang is with Department of Computer Science, Brunel University London, Uxbridge, Middlesex, UB8 3PH (email: kezhi.wang@brunel.ac.uk).

*These authors contributed equally to this work.

developed [12], [13]. Furthermore, bacteria can be a good choice for MC scene due to their inherent characteristics like quorum sensing (QS) [14]. For example, a QS-based theoretical MC system using bacteria as the transceivers is proposed in [15]. For bio-inspired MC system in [16], [17], bacteria are used as information carriers and QS is considered at the receiver. In [18], an externally controllable biological MC testbed using *Escherichia coli* (*E. coli*) bacteria is described. However, information carriers propagated in intricate channel environment are susceptible to interference (e.g., ISI, environmental noise) and prone to loss of control [19], resulting in greatly reduced transmission efficiency. To overcome this issue, the controllable electrophoretic force is utilized to propagate charged information-carrying molecules in MC systems, which is proposed in [20], [21]. As for bacteria, some of their motion characteristics like phototaxis and magnetotaxis also make external control possible by applying external stimuli [22], [23]. In [24], phototaxis is used to control the motion of microfabricated structures powered by flagellated bacteria. In [25], [26], the control strategy of magnetotactic bacterium (MTB) is proposed based on a magnetic manipulation system.

Recently, the magnetically-controlled micro-nano robot is one of the cutting-edge topics [27], and may have potential applications in the field of tumor targeted therapy in the future [28]. In addition, the idea of using MC theory to construct Internet of Bio-NanoThing (IoBNT) has been proposed firstly in [29], where bacteria populations are commonly used to relay the IoBNT information. IoBNT also has the potential applications in targeted therapy, and has received extensive discussion in recent years [30]–[32]. Motivated by above, a magnetotactic bacteria (MTB) based MC model is proposed in our work, which exhibits a combination of MC and magnetic controlled micro-nano robot. The magnetic control of MTB can contribute to mitigating ISI and improving the transmission efficiency in this MC system.

The second important difference between our approach and prior works is the network architecture applied for DL-based signal detection. In most existing DL-based MC literature, the RNN architectures, which are believed to have a good performance on temporal sequence processing, are applied for signal detection [5], [33]. For example, as a pioneering work, bidirectional long short term memory (BiLSTM) is proposed for signal detection, which shows better computationally efficiency and bit error rate (BER) performance than Viterbi detector with imperfect CSI as well as other DL-based detectors [5]. However, recent studies indicate that convolutional networks outperform recurrent architectures on a wide range of sequence modeling tasks, including audio synthesis and machine translation [34]. Motivated by this, instead of using RNN architectures, we propose a modified Temporal Convolutional Network (TCN) to perform signal detection with ISI effects.

Therefore, in this work, a modified TCN-based signal detection method for MTB communication system is proposed, utilizing MTB as information carriers. The straightforward Deep Neural Networks (DNN) and BiLSTM proposed in [5] are used for comparison. The motion of MTB in the channel is affected by both diffusion and magnetic drift. The dynamic

signal transduction of QS at the receiver is performed to achieve the diversity of information monitoring methods. In particular, both the observed signal with certain statistical information and QS signal with an unsolvable underlying model are considered. If the observed signal is the former one, the model-based detectors and DL-based detectors are executed to evaluate the system performance. However, if the observed signal is QS signal, only the DL-based detectors are performed and the universality of the proposed detectors is demonstrated.

The main contributions of this paper are summarized as follows:

- A magnetically-controlled MC system is proposed. This model utilizes the magnetotaxis and QS characteristics of MTB, which contributes to the controllability and reliability of typical DMC system.
- A modified TCN is proposed to recover transmitted sequences from observed signal. Specifically, the original TCN is modified as a bidirectional architecture to take the ISI effect into consideration.
- Two other DL-based approaches, DNN and BiLSTM, are considered for comparison. Also, the model-based optimal and sub-optimal MAP detectors are served as benchmarks when evaluating observed signal with certain statistical information. The BER performance of MTB communication system is evaluated on proposed approaches, including system parameters, complexity and robustness.

The rest of the paper is organized as follows. In Section II, the mathematical modeling of MTB communication system is described. In Section III, two model-based detectors based on MAP estimation method and DL-based detectors including TCN-based, BiLSTM-based and DNN-based detectors are presented. In Section IV, the BER performance evaluation for various detectors under MTB communication system is performed, followed by the concluding remarks in Section V.

II. MTB COMMUNICATION SYSTEM MODEL

A particular MC system, which uses MTB as information carriers, is considered in this work. As shown in Fig. 1, the MTB bacteria are stored in a bacteriological culture dish, which is then connected to the transmitting point, while the receiver stores some non-motile, nonmagnetic bacteria with flagella removed. At the start of each symbol slot, the switch of the bacteriological culture dish is turned on. The bacteria will be released instantaneously from the transmitting point through specific methods such as microfluidic technology and then propagate into the physical channel through flagella. In the channel, the movement of MTB is subjected to Brownian motion and magnetic drift, which is caused by the external magnetic force. The non-motile bacteria without magnetotaxis at the receiver are assumed to express the luminescent gene in response to the autoinducing molecules induced by the accumulation of MTB [15]. Specifically, once the density of MTB in the receiver region reaches a critical threshold, the non-motile bacteria begin to produce luminescence significantly through QS [35]. In this section, we will focus on the mathematical modeling of this communication system.

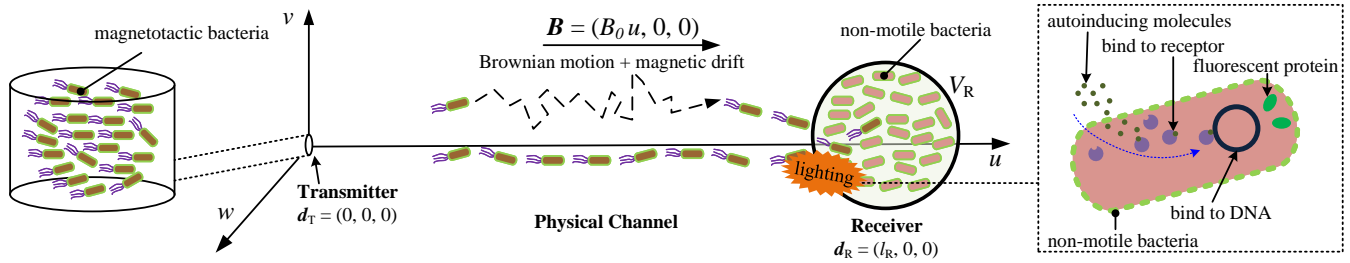


Fig. 1. MTB communication system in 3-D Cartesian coordinates. The locations of release point and receiver center are $\mathbf{d}_T = (0, 0, 0)$ and $\mathbf{d}_R = (l_R, 0, 0)$, respectively.

A. Transmitter Model

In typical communication systems, the information bits are required to be modulated and then be sent into the channel by the transmitter. Here, the On-Off Keying (OOK) modulation is adopted and the transmission time slot of each information bit is denoted by T_s . The modulation scheme of the transmitter can be expressed as:

$$n_T[k] = \begin{cases} N, x[k] = 1 \\ 0, x[k] = 0 \end{cases}, (k = 1, 2, \dots), \quad (1)$$

where $n_T[k]$ is the number of MTB released in the k th time slot, $x[k]$ is the k th symbol of transmitted sequence and N is a fixed value.

As shown in Fig. 1, we assume that the initial coordinate of all released bacteria is $\mathbf{d}_T = (0, 0, 0)$. Furthermore, processing time for release of MTB is not taken into account, indicating that the bacteria are released instantaneously.

B. Physical Channel Model

In the physical channel, the movement of MTB is affected by both Brownian motion and magnetic drift which is produced by external magnetic field. When an individual bacterium is placed in a magnetic field with a strength vector \mathbf{B} , the total magnetic force \mathbf{F}_m exerted on it can be calculated as [27]:

$$\mathbf{F}_m = (\boldsymbol{\mu} \cdot \nabla) \mathbf{B} = \left[\frac{\partial \mathbf{B}}{\partial u} \quad \frac{\partial \mathbf{B}}{\partial v} \quad \frac{\partial \mathbf{B}}{\partial w} \right]^T \boldsymbol{\mu}, \quad (2)$$

where $\boldsymbol{\mu}$ is magnetic moment of the bacterium and ∇ denotes hamiltonian operator. Assuming that the magnetic force on the bacterium is along u direction, the magnetic field is denoted as $\mathbf{B} = (B_0 u, 0, 0)$. In liquid with low Reynolds numbers, the bacterium would rapidly be accelerated to the terminal velocity $\mathbf{v}_m = \mathbf{F}_m / \zeta$ [36], where $\zeta = \frac{k_B T}{D}$ is the friction coefficient. Hence, we obtain the velocity of magnetic drift along u direction:

$$v_m = \frac{B_0 \mu D}{k_B T}, \quad (3)$$

where $k_B = 1.38 \times 10^{-23} \text{ J} \cdot \text{K}^{-1}$ is Boltzmann's constant, T is the temperature in kelvin and D is the diffusion coefficient of MTB. The motion of a bacterium in the channel is a Markov process [37], which can be discretized by a time period of

duration Δt [1]:

$$\begin{cases} (u_i, v_i, z_i) = (u_{i-1}, v_{i-1}, w_{i-1}) + (\Delta u_i, \Delta v_i, \Delta w_i) \\ \Delta u_i \sim \mathcal{N}(v_m \Delta t, 2D \Delta t) \\ \Delta v_i \sim \mathcal{N}(0, 2D \Delta t) \\ \Delta w_i \sim \mathcal{N}(0, 2D \Delta t) \end{cases}, \quad (4)$$

where coordinate (u_i, v_i, z_i) represents the position of the bacterium at time $t = i \Delta t$, $i = 1, 2, \dots$ and Δu_i , Δv_i , Δw_i are the random displacements during Δt . Since the magnetic drift velocity only exists along u direction, the mean of Δu_i is $v_m \Delta t$.

In MC, Fick's law is usually used to approximate the diffusion process of information carriers [1]. Here, let the vector $\mathbf{d}(t) = [u, v, w]$ represents the position of MTB in 3-D Cartesian coordinate at time t , as shown in Fig. 1. The combined effect of magnetic drift and Brownian motion is characterized by the derived *Probability Density Function* (PDF) [38], [39] of a MTB released by the transmitter:

$$f(\mathbf{d}, t) = \frac{1}{(4\pi Dt)^{3/2}} \times \exp\left(-\frac{\|\mathbf{d} - t\mathbf{v}_m - \mathbf{d}_T\|^2}{4Dt}\right). \quad (5)$$

C. Receiver Model

As shown in Fig. 1, we assume that the coordinate of the receiver center is $\mathbf{d}_R = (l_R, 0, 0)$, and the spherical receiver volume is V_R . The receiver is designed as a passive observer, so the capture probability of a bacterium in the receiver volume can be obtained by integrating (5). We assume that the receiver is far enough from the transmitter, then the $f(\mathbf{d}, t)$ of all points within the receiver volume can be approximated by its value at the center of the receiver according to the *Uniform Concentration Assumption* (UCA) [38]. Therefore, the capture probability at the receiver can be approximated as:

$$p(t) \approx \int_{\mathbf{d} \in V_R} f(\mathbf{d}_R, t) d\mathbf{d} = \frac{V_R}{(4\pi Dt)^{3/2}} \times \exp\left(-\frac{[l_R - v_m t]^2}{4Dt}\right). \quad (6)$$

Considering that the movement of each bacterium is independent, the number of bacteria observed at the receiver N_S follows a Binomial distribution when transmitter sends a single bit 1. Then, when parameter N is large and $p_{\text{isi}}(t)$ is sufficiently small (usually, in the case that $N \geq 20$ and $p_{\text{isi}}(t) \leq 0.05$, this condition can be considered to be met

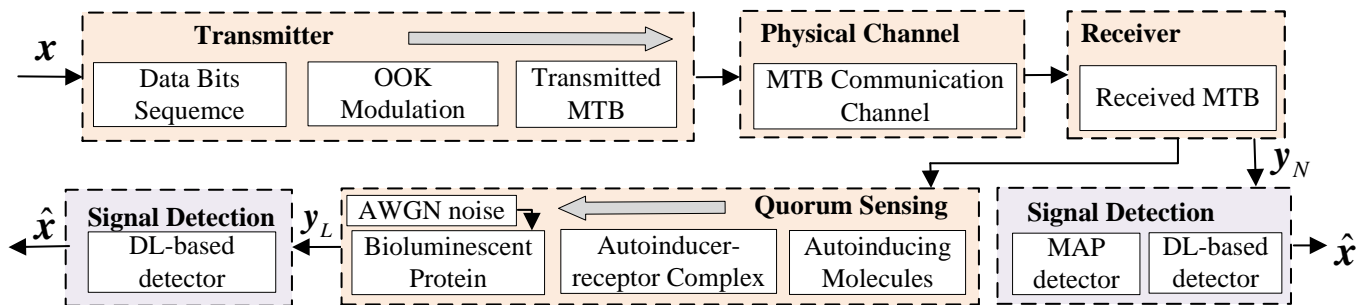


Fig. 2. Signal detection architecture for MTB communication system.

[40]), Binomial distribution can be well approximated as Poisson distribution with the same expected value:

$$N_S(t) \sim \mathcal{B}(N, p(t)) \sim \mathcal{P}(Np(t)). \quad (7)$$

In MC system, the effect of ISI is considered as a major source of impairment, which means that the received symbols would spread to adjacent symbols and smear into each other, especially when the system is stochastic, leading to the distortion of the received symbol in the current time slot [13]. Therefore, considering the ISI effect of independent m previous symbols, the number of bacteria observed at the receiver during the k th symbol time is expressed as:

$$N_R(k, t | \mathbf{x}_{k-m}^k) = \sum_{i=0}^m x[k-i] N_S(t - t_0 + iT_s) \quad (8)$$

$$t \in (t_0, t_0 + T_s],$$

where $t_0 = (k-1)T_s$, $\mathbf{x}_{k-m}^k = [x[k-m], \dots, x[k-1], x[k]]$. Note that in the case of $k-i \leq 0$, then $x[k-i] = 0$. For the independent Poisson random variable with parameter λ_i , $i \in [0, m]$, it can be proved that the sum of these random variables still obeys a Poisson distribution with parameters $\sum_{i=0}^m \lambda_i$ [41]. Therefore, the distribution of $N_R(k, t | \mathbf{x}_{k-m}^k)$ can be represented as:

$$N_R(k, t | \mathbf{x}_{k-m}^k) \sim \mathcal{P}(N p_{\text{isi}}(k, t | \mathbf{x}_{k-m}^k)), t \in (t_0, t_0 + T_s], \quad (9)$$

where $p_{\text{isi}}(k, t | \mathbf{x}_{k-m}^k) = \sum_{i=0}^m x[k-i] p(t - t_0 + iT_s)$. For a transmitted sequence with length n , we can obtain $N_R(t | \mathbf{x}_1^n)$ and $p_{\text{isi}}(t | \mathbf{x}_1^n)$ by splicing (8) and (9) from $k=1$ to $k=n$. Similarly, the distribution of $N_R(t | \mathbf{x}_1^n)$ can be represented as $N_R(t | \mathbf{x}_1^n) \sim \mathcal{P}(N p_{\text{isi}}(t | \mathbf{x}_1^n))$.

D. Quorum Sensing Process

The QS process [15] is considered and analysed in our MTB communication system, as shown in Fig. 1. Once the transmitted MTB arrive, the produced autoinducing molecules would initiate the transcription process of luminescent genes in non-motile bacteria at the receiver. The concentration of autoinducing molecules increases with the rising of MTB density, and the corresponding relationship is expressed as [42]:

$$\frac{dA}{dt} = v_A N_R - d_A A, \quad (10)$$

where A , v_A , and d_A are the concentration, the production rate and the degradation rate of autoinducing molecules, respectively. The autoinducing molecule then forms a complex with the bacterial cell receptor with probability $\rho(t)$, the dynamic of which is described as [35]:

$$\frac{d\rho}{dt} = -\kappa\rho + A\gamma(1-\rho), \quad (11)$$

where κ is the dissociation rate and γ is the complex formation rate. The concentration of autoinducing molecules would control the genetic expression of bioluminescent genes. That is, when the cell receptor binds to the autoinducing molecule, it activates the bioluminescent *lux* gene. The gene expression can be approximated by a two-step process [35]:

$$\begin{cases} \frac{dS}{dt} = (b_0\rho + a_0) - b_1 S \\ \frac{dL_0}{dt} = a_1 S - b_2 L_0 \end{cases}, \quad (12)$$

where L_0 is the number of bioluminescent protein, S is the number of post-transcriptional messengers, a_0 is the production of bioluminescent proteins in the absence of autoinducing molecule [43], b_0 is the rate of post-transcriptional messenger production, a_1 is the rate of fluorescence production, b_1 is the decay rate of post-transcriptional messengers, and b_2 represents the decay rate of fluorescence [16]. Here, additive white Gaussian noise (AWGN) is considered in the QS process:

$$L = L_0 + \epsilon_L, \quad (13)$$

where ϵ_L follows a Normal distribution $\epsilon_L \sim \mathcal{N}(0, \sigma_L^2)$.

III. SIGNAL DETECTION

The aim of signal detection is to accurately recover the transmitted bits from the observed signal. The architecture of the signal detection for the proposed MTB communication system is shown in Fig.2. In particular, we recover the transmitted sequence from two types of observed signals: the number of MTBs that arrived at the receiver region, denoted by \mathbf{y}_N , and the luminescence intensity, denoted by \mathbf{y}_L . The probability distribution information of \mathbf{y}_N is derived in equation (9), but \mathbf{y}_L has no definite distribution information because of the complex consecutive stochastic processes. In this section, we propose two model-based detectors based on MAP estimation method for signal \mathbf{y}_N and DL-based detectors for both signals \mathbf{y}_N and \mathbf{y}_L .

A. Model-based MAP Detector

Let $\mathbf{y}_N[k]$ be the signal observed by receiver in the k th symbol slot and $\hat{x}[k]$ be the symbol that is estimated for the k th transmitted symbol $x[k]$. Assuming synchronous transmission, the receiver counts the number of MTBs multiple times within each symbol interval, with a sampling interval of t_a . Thus, the signal observed by the receiver in the k th symbol slot, denoted as $\mathbf{y}_N[k]$, can be represented as:

$$\mathbf{y}_N[k] = [N_R(t_0 + t_a), N_R(t_0 + 2t_a), \dots, N_R(t_0 + at_a)], \quad (14)$$

where $t_0 = (k-1)T_s$, and a is the number of sampling points denoted as $a = \frac{T_s}{t_a}$. To reduce the bit error rate (BER), error correction coding methods such as convolutional codes and repetition codes can be applied to the source signal. However, for the sake of generality, we do not consider these methods here. The BER can be directly calculated based on the transmitted symbols $x[k]$ and the estimated ones $\hat{x}[k]$.

The optimal MAP detector considers all possible transmitted sequences and selects the one that maximizes the posterior expected value of the observed signal. In this work, we assume that the prior probability of the transmitted sequence follows a uniform distribution. The optimal MAP detector can be represented by Bayes rules as [44]:

$$\hat{\mathbf{x}}_1^n = \arg \max_{\mathbf{x}_1^n} f_{\text{model}}(\mathbf{y}_N^n | \mathbf{x}_1^n; \Theta), \quad (15)$$

where f_{model} is the relationship between the transmitted sequence and the observed signal, n is the length of transmitted sequence, $\mathbf{y}_N^n = [\mathbf{y}_N[1], \mathbf{y}_N[2], \dots, \mathbf{y}_N[n]]$ and Θ is the model parameter sets.

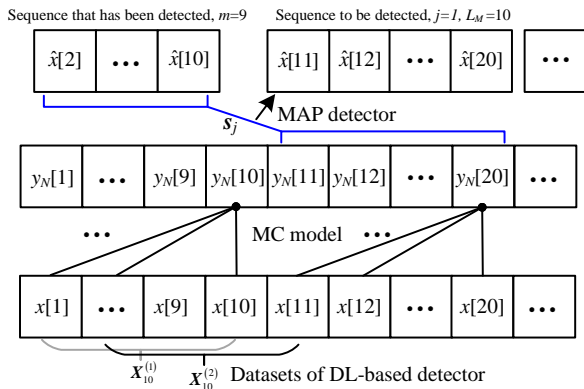


Fig. 3. Datasets of DL-based detector and signal detection based MAP detector for $n > 20$, $m = 9$, $L_M = 10$, $l = 10$ and $j = 1$.

To simplify calculation, we just consider one sampling point of the observed signal to detect $\hat{x}[k]$ through MAP detector. The $\mathbf{y}_N[k]$ in (14) then becomes a scalar $y_N[k] = N_R(kT_s)$. It is obvious that the computational complexity of the optimal MAP detector is $O(2^n)$, which is not applicable when n is large and would affect the real-time performance of signal detection. In order to reduce the computational complexity, we separate the signal sequence into multiple groups, and the sequence length of each group is set to L_M . In this way, the computational complexity of MAP detector can be reduced to $O(\frac{n}{L_M} 2^{L_M})$. However, the separated sequence groups are not

independent due to the ISI effect. Therefore, when detecting each group of sequences, the detection result of previous m symbols is used as a condition of MAP, which can be represented as:

$$\hat{\mathbf{x}}_{j+1}^{j+L_M} = \arg \max_{\mathbf{x}_{j+1}^{j+L_M}} f_{\text{model}}(\mathbf{y}_N_{j+1}^{j+L_M} | \mathbf{s}_j; \Theta), \quad (16)$$

where $j = (0, L_M, 2L_M, \dots)$ is the index of groups, $\mathbf{s}_j = [\hat{\mathbf{x}}_{j-m}^j, \mathbf{x}_{j+1}^{j+L_M}]$ is a specific sequence for each group which combines detection result of previous m symbols and sequence to be detected. Suppose MAP detector can fully extract the mathematical model in Section II, so the distribution of $\mathbf{y}_N_{j+1}^{j+L_M}$ is $N_R(t | \mathbf{s}_j) \sim \mathcal{P}(Np_{\text{isi}}(t | \mathbf{s}_j))$, where $t = (j+1)T_s, \dots, (j+L_M)T_s$. Finally, equation (16) can be reorganized as:

$$\hat{\mathbf{x}}_{j+1}^{j+L_M} = \arg \max_{\mathbf{x}_{j+1}^{j+L_M}} \prod_{k=j+1}^{j+L_M} \frac{(Np_{\text{isi}}(kT_s | \mathbf{s}_j))^{N_R(kT_s | \mathbf{s}_j)} \exp(-Np_{\text{isi}}(kT_s | \mathbf{s}_j))}{N_R(kT_s | \mathbf{s}_j)}. \quad (17)$$

As shown in Fig. 3, each observed signal is dependent on the corresponding transmitted symbol and the previous symbols (we set $m = 9$ in this paper). Therefore, we regard the case of $L_M = m + 1 = 10$ as an approximate optimal MAP detector, and the computational complexity of which is $O(\frac{n}{10} 2^{10})$. Furthermore, we regard the case of $L_M = 1$ as a sub-optimal MAP detector, and the computational complexity of which is down to $O(2n)$.

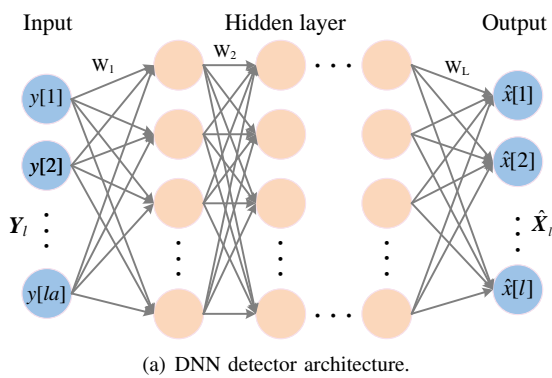
B. DL-based Signal detector

In Section III-A, we propose the optimal and sub-optimal model-based MAP detectors for signal detection, assuming known model parameters. However, in practical MC systems, it is difficult to model the communication system and parameter distribution completely and precisely. Many detection algorithms estimate system parameters by sending pilot symbols, which results in extra overhead [45]. Next, we will focus on the DL-based signal detection methods, which do not require the underlying modeling information in detail.

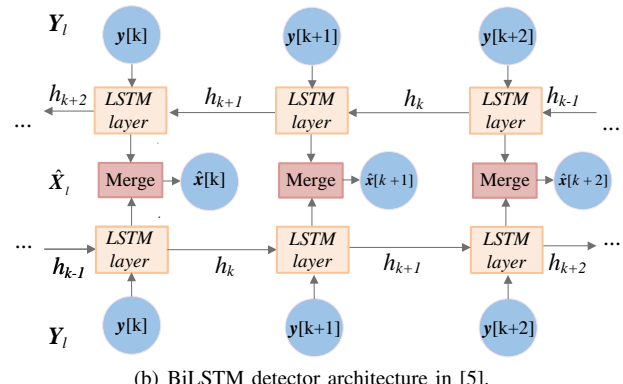
DL-based detection methods typically involve two phases. In the first phase, datasets extracted from the simulation process of the MC system are used for offline training of DL networks. In the second phase, when the networks are well trained with satisfactory training and testing accuracy, they can be deployed and used for signal detection.

Let $\mathbf{X}_l^{(k)} = [x[k], x[k+1], \dots, x[k+l-1]]^T$ be a sequence of l transmitted symbols beginning at index k , and $\mathbf{Y}_l^{(k)} = [\mathbf{y}_N[k], \mathbf{y}_N[k+1], \dots, \mathbf{y}_N[k+l-1]]^T$ or $[\mathbf{y}_L[k], \mathbf{y}_L[k+1], \dots, \mathbf{y}_L[k+l-1]]^T$ be the corresponding observed signal. Note that $\mathbf{X}_l^{(k)}$ and $\mathbf{Y}_l^{(k)}$ have dimensions of $l \times 1$ and $l \times a$, respectively. As shown in Fig. 3, the sliding window processing method is performed on the original data progressively to obtain datasets similar to [5], which are represented by:

$$\left\{ \left(\mathbf{X}_l^{(1)}, \mathbf{Y}_l^{(1)} \right) \left(\mathbf{X}_l^{(2)}, \mathbf{Y}_l^{(2)} \right) \dots \left(\mathbf{X}_l^{(n-l+1)}, \mathbf{Y}_l^{(n-l+1)} \right) \right\}, \quad (18)$$



(a) DNN detector architecture.



(b) BiLSTM detector architecture in [5].

Fig. 4. Neural network detectors for comparison.

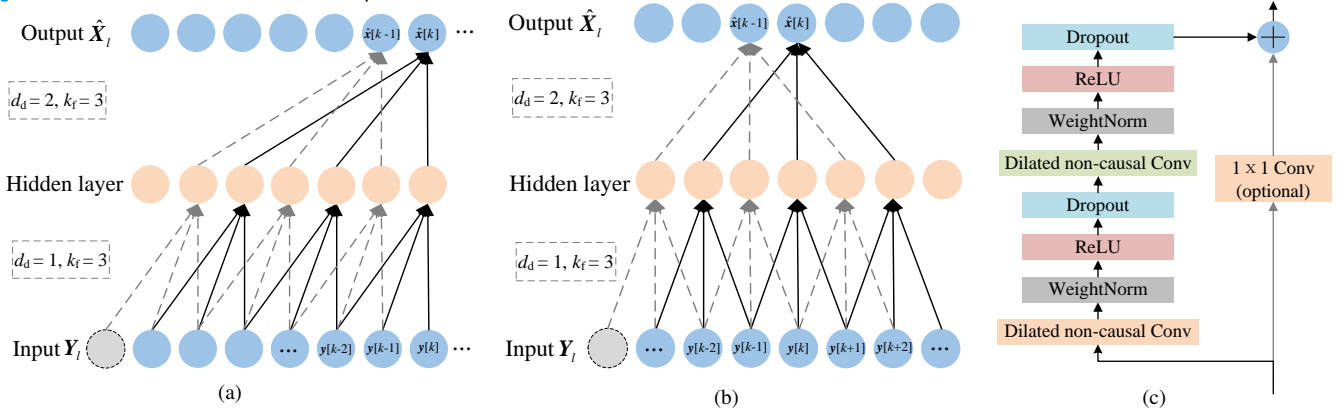


Fig. 5. TCN detector architecture. (a) Dilated causal convolutions diagram for dilation factors $d_d = 1, 2$ and filter size $k_f = 3$. (b) Dilated non-causal convolutions diagram for dilation factors $d_d = 1, 2$ and filter size $k_f = 3$. (c) TCN residual block [34].

where $(\mathbf{X}_l, \mathbf{Y}_l)$ is a transmit-receive sequence pair composed of l consecutive transmissions.

With the achieved datasets, a specific predesigned DL network would be employed at the receiver to train a classifier. The input of DL network is the observed signal \mathbf{Y}_l and output is the estimation of transmitted symbols $\hat{\mathbf{X}}_l$. During the training process, the optimal set of network parameters \mathcal{W}^* which leads to the minimum value of the loss function \mathcal{L}_{loss} would be obtained gradually with the gradient descent algorithm. This process is represented as:

$$\begin{aligned} \mathcal{W}^* &= \arg \min_{\mathcal{W}} \mathcal{L}_{loss}(\mathbf{X}_l, \hat{\mathbf{X}}_l) \\ &= \arg \min_{\mathcal{W}} \sum_{i=1}^l \mathcal{H}((x[i], \hat{x}[i])), \end{aligned} \quad (19)$$

where \mathcal{H} is the cross entropy between the real transmitted and estimated symbols. Minimizing the loss function is equivalent to maximizing the log-likelihood function using Bayes' theorem [46]. Therefore, DL-based detection methods can be seen as building on the theoretical baseline of MAP estimation, which fully grasps the model parameters.

As shown in Fig. 2, we evaluate different DL-based detectors on both observed signals \mathbf{y}_N and \mathbf{y}_L . Specifically, TCN is introduced, and another two DL-based networks, denoted as DNN and BiLSTM, are analysed as well for comparison. Also, the model-based MAP detectors proposed in Section III-A is considered as benchmarks. It should be noted that for BiLSTM and TCN-based detectors, the input data has one more dimension than that for DNN, which is known as encoding vector in natural language processing [47]. Since

the input data \mathbf{Y}_l is an $l \times a$ matrix, each observation signal of single symbol $\mathbf{y}[k]$ can be set as a encoding vector. For DNN-based detector, $\mathbf{y}[k]$ is required to flatten into a scalar because DNN has no dimension of encoding vector. Then, the input data of DNN-based detector is converted to $\mathbf{Y}_l = [y[1], y[2], \dots, y[la]]^T$ with length la .

1) *DNN-based Detector*: Fig. 4(a) shows the architecture diagram of DNN, where \mathbf{Y}_l and $\hat{\mathbf{X}}_l$ represent the input and output vector respectively, and W_j stands for the weight matrix of the j th hidden layer. Because DNN does not have memory modules like LSTM and TCN, it may not be able to effectively capture long-term dependencies in the input data. This can result in reduced performance when processing data with severe inter-symbol interference (ISI) effect, which can introduce complex dependencies between adjacent symbols.

2) *BiLSTM-based Detector*: Without knowing the communication system model and its parameters, N. Farsad et al [5] proposes to use BiLSTM networks detector for signal detection. The received signal sequence can be fed forward to one RNN layer and backward to another RNN layer simultaneously, and then the outputs of the two LSTM layers are merged [48], as shown in Fig. 4(b). This architecture ensures that future observations are taken into account when estimating the current symbols.

3) *Modified TCN-based Detector*: S.Bai et al. [34] believe that RNN architecture like LSTM is outdated, and convolutional architecture should be considered as one of the main candidates for processing sequence data. In this work, we propose a modified convolutional architecture based detector, denoted as TCN, for signal detection in the MTB communi-

TABLE I
THE DEFAULT VALUES OF SIMULATION PARAMETERS

Transmitter & Physical Channel & Receiver				Quorum Sensing			
parameter	value	parameter	value	parameter	value	parameter	value
N^*	10^5	T_s^*	4s	γ	$0.8 \times 10^{-4} (\text{nM} \cdot \text{s})^{-1}$	κ	0.5s^{-1}
D	$7.5 \times 10^{-10} \text{m}^2 \cdot \text{s}^{-1}$	T	300K	v_A	$0.8 \text{nM} \cdot \text{s}^{-1}$	d_A	0.5s^{-1}
r_R^*	$6.7 \mu\text{m}$	μ	$1 \times 10^{-16} \text{A} \cdot \text{m}^2$	a_0	0s^{-1}	b_0	0.8s^{-1}
B_0^*	$1 \text{mT} \cdot \text{mm}^{-1}$	m	9	a_1	0.8s^{-1}	b_1	0.5s^{-1}
l	$100 \mu\text{m}$			σ_L^*	0	b_2	0.5s^{-1}

* Parameters that may vary when generating specific datasets.

tion system. The schematic diagram of TCN architecture based on causal convolution, proposed in [34], is shown in Fig. 5(a). Note that the dilated factor d_d in TCN is used to introduce a fixed window between every two adjacent convolution filters. By introducing the dilated factor, the receptive field of historical data can be greatly expanded, which is expected to improve the network performance when tackling time sequence tasks that require a long memory. However, similar to BiLSTM-based detectors, signal detection based on TCN also needs to consider a portion of future signal observations due to the influence of ISI effects. Therefore, unlike the original causal convolution proposed in [34], we expand the receptive field to cover part of the future data, as shown in Fig. 5(b). In addition, to guarantee the stability of deeper and larger TCN, the residual block [49] is also used in our TCN-based detector, as displayed in Fig. 5(c).

IV. RESULTS AND DISCUSSION

In this work, a modified TCN-based detector is proposed for signal detection, and DNN and BiLSTM used in [5] are applied as well for comparison. Meanwhile, the optimal and sub-optimal MAP detectors will serve as the theoretical baselines for DL-based signal detection when estimating y_N . In this section, a series of experiments are operated to evaluate the performance of proposed detectors. In particular, the process of dataset generation is first declared in Section IV-A. Then the effect of sampling number and training sequence length on BER performance is evaluated, and the optimal values of corresponding parameters used for subsequent experiments are determined in Section IV-B. In Section IV-C, the comparison of model complexity for proposed detectors with different number of neurons is conducted to ensure a fair comparison between different schemes. Furthermore, Section IV-E evaluates the effect of emitted bacteria number N , symbol slot T_s and magnetic field gradient B_0 on BER performance. Finally, Section IV-D provides the robustness analysis for DL-based detectors when estimating y_L by introducing AWGN noise to the test set for BER evaluation.

A. Datasets Generation

The default values of simulation parameters are given in Table I. Among them, the magnetic moment m and diffusion coefficient D are determined according to [50] and [51] respectively. The number of symbols considered in ISI effect is set to $m = 9$, and the influence of more previous symbols is ignored. The value of other parameters is selected to satisfy

the assumptions in the theoretical model derived above. Note that parameters marked with an asterisk (*) may vary in some cases, which will be illustrated significantly.

First, to verify the accuracy of equation (6), we conduct the particle-based simulation through equation (4) by tracking the movement of all MTB sent by transmitter. Then the number of MTB which enter the spherical receiver region, denoted as simulated N_R , is recorded. Fig. 6 shows the comparison results of simulated N_R and mathematically derived N_R expectation (which equals $N \times p(t)$), where the black curve is the average result of ten simulated N_R sets. If the parameter values are set to $r_R = 25 \mu\text{m}$, $l_R = 100 \mu\text{m}$, it will be found that $N \times p(t)$ does not fit the average value of multiple simulated N_R sets well. However, if we set $r_R = 6.7 \mu\text{m}$, $l_R = 100 \mu\text{m}$, it can be seen that $N \times p(t)$ can fit the average value of multiple simulated N_R sets, which means that default parameters, including diffusion coefficient, drift velocity, etc., in Table I are sufficient to meet the UCA assumptions, and the mathematical model can accurately represent the motion process of MTB in the channel.

Next, we will show the data generation process of MTB communication system from the emission of data bits to final production of luminescence protein. A data bits sequence is first randomly generated, e.g., $\mathbf{x} = [1, 0, 1, 1, 0, 0, 1, 1, 0, 0]$, followed by the generation of N_R according to equation (9). Each transmitted symbol $x[k]$ from the data bits sequence corresponds to a $1 \times a$ vector $\mathbf{y}_N[k] = [N_R(t_0 + t_a), N_R(t_0 + 2t_a), \dots, N_R(t_0 + at_a)]$, where k is the index of transmitted symbol and $t_0 = (k - 1)T_s$. In most MC literature, N_R is considered as the observed signal to estimate transmitted symbols. Fig. 7(a) shows the data generation result of N_R , and a relatively large oscillation can be easily observed which indicates the Poisson channel noise in equation (9).

Since the input N_R is a random process function with uncertainty, it is difficult to directly obtain the analytical expression of these differential equations. In order to describe the QS process more clearly, the differential equations (10), (11) and (12) are numerically simulated. For instance, equation (10) is discretized as follows:

$$\frac{A(t + \Delta t) - A(t)}{\Delta t} = v_A N_R(t) - d_A A(t), \quad (20)$$

where Δt is time resolution of generated data. Equations (11) and (12) are discretized in a similar way, where the final results are shown in Fig. 7(a) and Fig. 7(b). In this work, in addition to the received number of MTB in the receiver region, we also consider the luminescence intensity

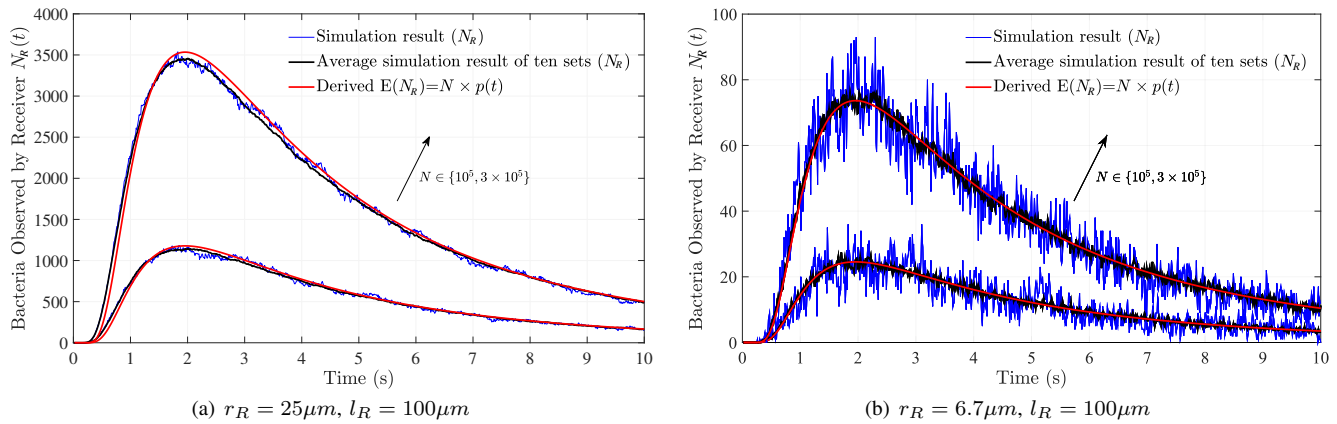


Fig. 6. Simulation results of N_R by equation (4) and $Np(t)$ for $N \in \{10^5, 3 \times 10^5\}$.

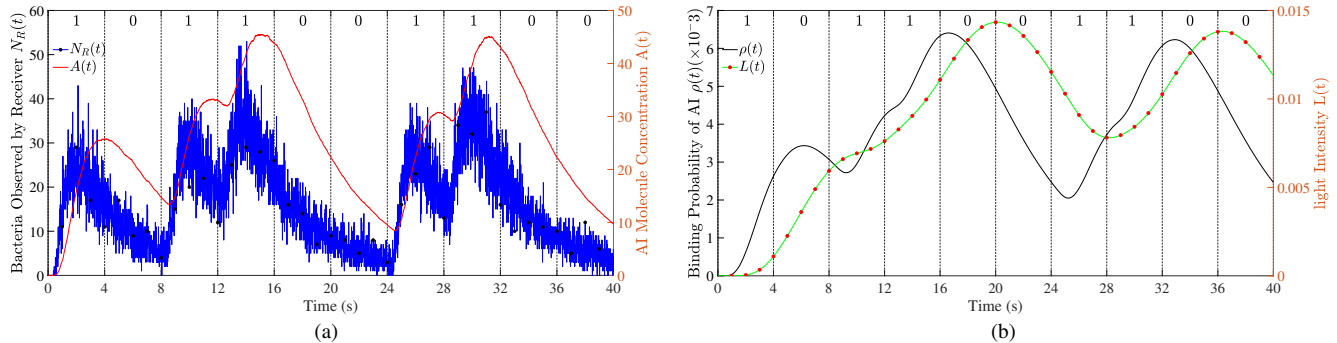


Fig. 7. Data generation result when data bits sequence $x = [1, 0, 1, 1, 0, 0, 1, 1, 0, 0]$. (a) The number of bacteria observed by spherical receiver N_R and autoinducing molecule concentration A . The black spot is sampling point for N_R in the case of $a = 4$. (b) The probability $\rho(t)$ of autoinducing molecule forms a complex with the bacterial cell receptor and the fluorescence intensity L . Red spot is the sampling point for L in the case of $a = 4$.

L as another scheme of observed signal design through the QS process. Similarly, each transmitted symbol $x[k]$ of the data bits sequence corresponds to a $1 \times a$ vector $\mathbf{y}_L[k] = [L(t_0 + t_a), L(t_0 + 2t_a), \dots, L(t_0 + at_a)]$. From Fig. 7(a) and Fig. 7(b), we can find that the uncertainty disappears when N_R is transformed into the signal L , which is beneficial to improve the accuracy of signal recovery. Moreover, compared with the signal N_R , the signal L is more convenient to achieve in practical scenarios through devices such as the photomultiplier.

Specific data preprocessing techniques are required to enable the DL algorithms to process datasets. In this work, the dataset is generated where $n = 50000$ and test set is generated where $n = 10000$. The form of the dataset has been given by equation (18). Furthermore, min-max scaling is adopted for data normalization:

$$y^* = \frac{y - y_{min}}{y_{max} - y_{min}}, \quad (21)$$

where y^* is the normalized value, y_{min} and y_{max} represent the maximum and minimum value in the dataset respectively. Then the dataset is split into a training set and validation set, the ratio of which is 0.8 and 0.2 respectively.

B. Sampling Number and Sequence Length Analysis

The network architectures of different detectors based on TCN, BiLSTM and DNN are illustrated in Table II, and number of neurons of each layer are determined according to Section IV-C. The TCN residual block is illustrated in Fig. 5(b) and Fig. 5(c), where the filter size is set to $k_f = 3$ to

increase the receptive field of the detector. The cross entropy displayed in equation (19) is used as the loss function, and Adam algorithm is adopted as the gradient descent optimizer for all networks. The output of each layer in TCN, BiLSTM and DNN are 5, 5 and 60 respectively.

TABLE II
NEURAL NETWORK ARCHITECTURE

TCN	BiLSTM	DNN
Output($l, 1$)	Output($l, 1$)	Output(l)
TCN residual block($l, 5$)	BiLSTM($l, 5$)	Dense(60)
TCN residual block($l, 5$)	BiLSTM($l, 5$)	Dense(60)
Input(l, a)	Input(l, a)	Input(la)

¹ The filter size in TCN residual block is $k_f = 3$.

Next, in order to compare the performance between DL-based detector and MAP detector, we first analyze the dataset whose observed signal is \mathbf{y}_N . It is obvious that with the sampling number a increasing, more information can be obtained by the detector for each time slot. Here, we set the sequence length l of datasets as 1, so that each training sample only contains signal from one symbol slot. Fig. 8(a) shows the BER performance for different sampling numbers a . This indicates that when sampling number during each time slot is sufficient, e.g. $a = 20$, the performance of DNN-based detector, BiLSTM and TCN-based detectors are all perfect, which can reduce BER to 0. When the number of sampling points is reduced to $a \leq 2$, the observation information is insufficient and can be severely disturbed by ISI effect, leading to reduced

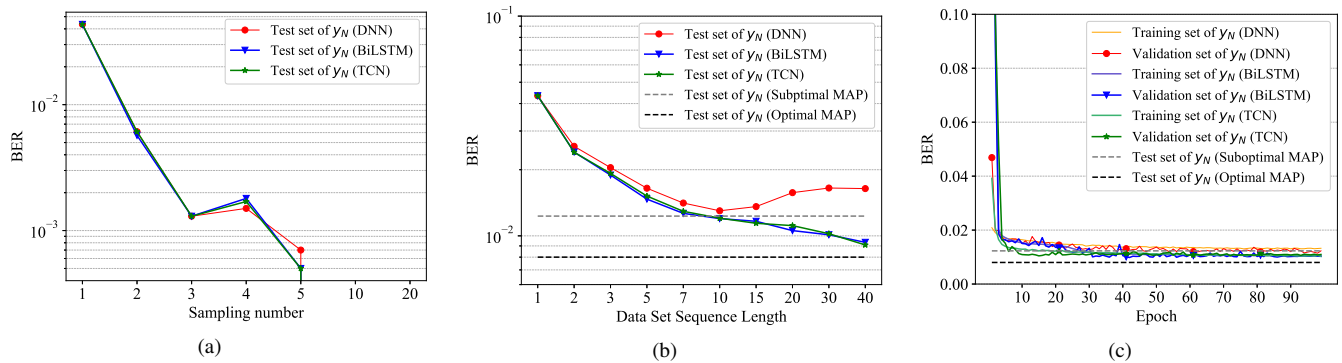


Fig. 8. The BER performance comparison of TCN, BiLSTM, DNN and MAP detector. (a) Effect of sampling number α for $l = 1$. (b) Effect of data set sequence length l for $\alpha = 1$. (c) The training process for $\alpha = 1$ and $l = 20$.

performance for all DL-based detectors.

In addition, the impact of transmit-receive sequence length l on the BER performance is shown in Fig. 8(b). With the increase of l , the performance of the TCN-based detector approaches that of the BiLSTM-based detector, but it is significantly better than that of the DNN. When the sequence length $l > 10$, the performance of TCN and BiLSTM surpasses that of the sub-optimal MAP detector, but DNN does not. When the sequence length $l = 40$, the performance of TCN and BiLSTM is close to the optimal MAP detector, but the performance of DNN becomes worse. The continuous increase in sequence length makes DNN detectors fall into overfull features and cannot accurately capture the dependencies of time sequence data like ISI. Also, this phenomenon reflects advantage of TCN and BiLSTM in extracting the ISI feature of time sequence data. Fig. 8(c) shows the training process for $\alpha = 1$ and $l = 20$, and we can clearly see that the whole training process converges stably and there is no obvious overfitting phenomenon. Due to space constraints, we do not show the training process for other parameters.

To conclude, when there are sufficient sampling points, all detectors can perform signal recovery well, making further comparison between them invalid. Meanwhile, MAP detector is analysed when sampling number $\alpha = 1$, so we choose $\alpha = 1$ for subsequent evaluations. Additionally, as the sequence length increases, the TCN and BiLSTM detectors outperform the sub-optimal MAP detector and approach the performance of the optimal MAP detector. However, the performance of the DNN detector is worse than that of the sub-optimal MAP detector. To facilitate better comparison, we will use a sequence length of $l = 40$ for subsequent evaluations.

C. Model Complexity Analysis

Since the network architecture of our detectors is artificially constructed, the internal layers and hyperparameters are required to be tuned according to the performance to determine an optimal value. For MC scenario, due to the size and limited capabilities of nano nodes, the complexity analysis is quite critical. Thus, we will analyze the model complexity from two aspects: training complexity and computational complexity.

Training complexity includes space complexity and time complexity, which is a measure of the model complexity during offline training. The space complexity of detector is

reflected by trainable parameters, and the time complexity is reflected by training speed. Trainable parameters are parameters that will be learned by DL model during training procedure including, e.g. weights and biases. Training speed is represented by the time used for each training epoch under the same batch size. Here, the number of neurons is considered for a overall comparison during evaluation, and the determination method for other hyperparameters is similar.

From our evaluation result shown in Fig. 9(a), the 60-neuron DNN-based detector can reduce the BER to 1.633%, which performs better than the 45, 75, 90-neuron detectors. If the number of neurons continues to increase, the number of trainable parameters will also increase, leading to an increase in space complexity. Therefore, the 60-neuron DNN is chosen as the final architecture for the DNN detector for subsequent comparisons.

Fig. 9(b) shows the evaluation result of BiLSTM-based detector. It can be seen that 5-neuron BiLSTM detector has the best performance, with the BER of 0.934%. However, the number of trainable parameters increases rapidly with the rising of neurons. Although the output of each BiLSTM layer is 5, while that of DNN is 60, 5-neuron BiLSTM-based detector still exhibits slower trainable speed than 60-neuron DNN-based detector. Thus we believe that the intricacy of the LSTM unit and bidirectional structure in BiLSTM-based detector may be the main reason for the higher time complexity. The 5-neuron BiLSTM is chosen as the final architecture of BiLSTM detector for comparison.

Then, the evaluation result of TCN-based detector is shown in Fig. 9(c). The graph shows that the 5-neuron TCN-based detector achieves the best BER performance, reaching 0.909%. Meanwhile, because the TCN architecture is simple, both the space and time complexity of 5-neuron TCN-based detector is lower than that of 5-neuron BiLSTM-based detector. In addition, compared to 60-neuron DNN-based detector, the training speed of 5-neuron TCN-based detector is slightly slower, but the BER performance and space complexity is much better. The 5-neuron TCN is chosen as the final architecture of TCN detector for comparison.

Computational complexity is a measure of model complexity for online signal detection, and we conduct a simple theoretical analysis here. Let l be the sequence length of each sample in the dataset. The computational complexity of DL-

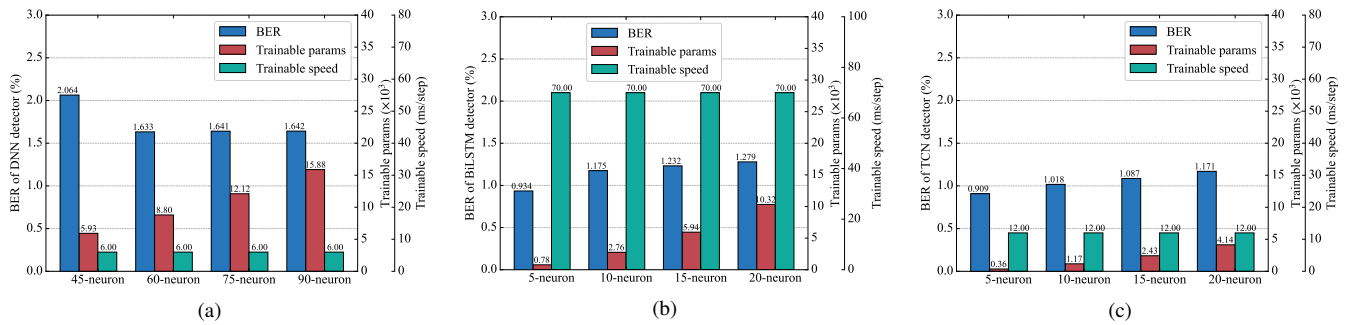


Fig. 9. The BER performance, trainable parameters and trainable speed comparison of TCN, BiLSTM, DNN detector. (a) DNN detectors with different neurons. (b) BiLSTM detectors with different neurons. (c) TCN detectors with different neurons.

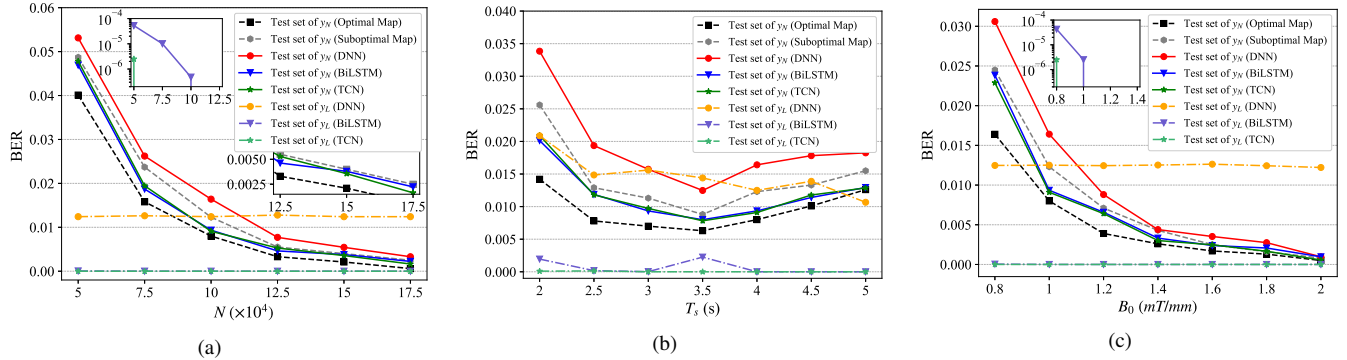


Fig. 10. The BER performance of TCN, BiLSTM, DNN and MAP detector. (a) Effect of channel noise represented by N . (b) Effect of symbol slot T_s . (c) Effect of magnetic field gradient B_0 .

based detectors can be expressed as $O(nl)$, while that of the MAP detector is $O(\frac{n}{L_M} 2^{L_M})$. Obviously, the computational complexity of MAP detector increases exponentially with L_M . In other words, the computational complexity of the optimal MAP detector is higher than that of DL detector. The sub-optimal MAP detector has lower computational complexity because L_M is set to 1, but both TCN and BiLSTM-based detectors outperform it, even though it completely grasps the channel information.

To conclude, with similar parameter settings, the BiLSTM and TCN-based detectors achieve better BER performance than DNN. However, considering both training and computational complexities, the TCN-based detector shows the best performance, since BiLSTM detector with same BER performance tends to require higher space and time complexity, which is a limitation for MC scenarios. It is important to note that the MAP detector assumes complete knowledge of channel information, but in practical cases, extra steps are needed to estimate the information parameters. Therefore, the optimal performance of MAP detector can only be achieved theoretically."

D. Intrinsic Channel Characteristics Analysis

In this section, we analyze the intrinsic influencing factors of the communication channel, including the number of bacteria emitted per symbol slot N , the symbol slot duration T_s , and the magnetic field gradient B_0 . We consider the BER performances of the DL-based detectors for both observed signals, y_N and y_L .

The effect of N on the BER performance is first evaluated, and the result is shown in Fig. 10(a). Here, we insert a

logarithmic sub-coordinate to show the BER of y_L during low BER regions to better compare the performance of detectors. The channel noise is affected by the parameter N . For a typical communication system, the signal-to-noise ratio (SNR) is usually applied to express the ratio of signal power to the noise power. The distribution of $N_R(t | x_1^n)$ is represented in Section II-C as $N_R(t | x_1^n) \sim \mathcal{P}(Np_{\text{isi}}(t | x_1^n))$, so the channel SNR [38] in MTB communication system is represented by:

$$\begin{aligned} \text{SNR}_{\text{CHANNEL}} &= 10 \log_{10} \left(\frac{\mathbb{E}(N_R(t | x_1^n))^2}{\text{Var}(N_R(t | x_1^n))} \right) \\ &= 10 \log_{10}(Np_{\text{isi}}(t | x_1^n)). \end{aligned} \quad (22)$$

It is clear that the channel SNR is proportional to N . When the observed signal is y_N , we find that the performance of DL-based detectors and MAP detector drops rapidly as N decreases, which indicates the increasing of the channel noise. Meanwhile, the BER performance of both TCN and BiLSTM-based detectors is better than the sub-optimal MAP and DNN-based detector, but worse than optimal MAP detector. When the observed signal is y_L , the TCN and BiLSTM-based detectors can achieve zero BER except for two points, while DNN-based detector has a large BER and does not change with N .

Next, the parameters in Table II have been reset and the impact of symbol duration T_s on the BER performance for all detectors is evaluated, as shown in Fig. 10(b). When the observed signal is y_N , we find that the performance of all detectors first decrease and then increases with the increase of symbol slot T_s . It can be seen from Fig. 6 that around $T_s = 2s$, the ISI effect is the most obvious, accompanied by large channel noise, so BERs of all detectors are high at this point.

As the symbol slot T_s increases, the ISI effect will decrease. However, with T_s continuously increasing, the difference of observed signals between bit 1 and bit 0 will gradually become tiny, causing the BER of all detectors to increase again. In addition, the BER of TCN and BiLSTM-based detectors are still better than the sub-optimal MAP and DNN-based detector, but worse than the optimal MAP detector. When the observed signal is \mathbf{y}_L , the TCN-based detector can basically achieve zero BER, whereas the BiLSTM-based detector is slightly less stable and the DNN-based detector has the worst performance.

In order to reduce the ISI effect to improve communication efficiency, the magnetic field gradient B_0 is further analysed. Fig. 10(c) shows that when the observed signal is \mathbf{y}_N , there is a strong correlation between B_0 and the ISI component. As B_0 increases, the ISI effect decreases, resulting in a decrease in BER. When B_0 increases to $2mT \cdot \text{mm}^{-1}$, the BER performance of all detectors is quite close because the ISI effect between symbols is negligible in this case. Furthermore, the BER of TCN and BiLSTM-based detectors remains better than the sub-optimal MAP and DNN-based detector, but worse than the optimal MAP detector. When the observed signal is \mathbf{y}_L , the TCN and BiLSTM-based detectors can almost achieve zero BER, while DNN-based detector has a large BER and does not change with B_0 .

If the observed signal is \mathbf{y}_L , both the TCN-based and BiLSTM-based detectors achieve zero BER in some cases. This phenomenon occurs because the introduction of QS process removes uncertainty in \mathbf{y}_N , and both the TCN-based and the BiLSTM-based detectors are very good at dealing with time sequence data. By contrast, the DNN-based detector is affected by interference of overfull features, resulting in getting stuck in local optimum points and losing the capability of accurately capturing the dependency of the time sequence data. Therefore, the DNN-based detector does not achieve zero BER like TCN-based and BiLSTM-based detectors. Moreover, the BER of DNN-based detector in Fig. 10(a) and Fig. 10(c) does not change with increasing N and B_0 . It can be inferred that the local optimum point DNN falls into is not sensitive to parameters N and B_0 , but is more sensitive to parameter T_s . This phenomenon also demonstrates the universality of TCN and BiLSTM-based detectors in signal detection.

E. Model Robustness Analysis

In order to simplify the process of external interference, AWGN is considered in \mathbf{y}_L in equation (13), which can be represented as:

$$\text{SNR}_{\text{AWGN}} = 10 \log_{10} \left(\frac{L_0^2}{\sigma_L^2} \right). \quad (23)$$

To further evaluate the robustness of the DL-based detectors, the optimal models achieved in Section IV-C are considered and tested on the dataset with different SNRs. The results are shown in Fig. 11. It is obvious that the BER performance of all detectors inevitably decreases with the increasing of SNR. Meanwhile, the BER performance of all DL-based detectors is not catastrophically broken when applied on the test set with Gaussian noise. In other words, the DL-based detectors

have a certain degree of robustness for additive Gaussian noise. Specifically, the proposed TCN-based detector shows the best robustness, with the least decline in BER performance compared to other detectors. Therefore, the proposed TCN-based detector in this work is believed to have advantages over other DL-based detectors in communication environment which is susceptible to external interference.

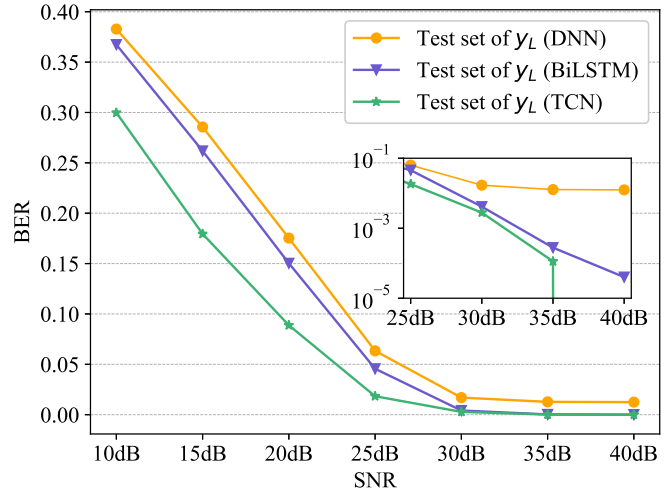


Fig. 11. The BER performance of TCN, BiLSTM, DNN and MAP detector on testing set with AWGN. The sub-coordinate is in logarithmic format to have better illustration for beyond 25 dB SNRs.

V. CONCLUSIONS AND FUTURE WORK

In this paper, a modified TCN-based detector is proposed for signal detection in MTB communication system, which uses MTB as information carriers to fully take advantages of magnetotaxis and QS characteristics of bacteria. The information transmission process of system shows that the introduction of magnetic drift can suppress ISI effect and improve communication efficiency. Two other DL-based detectors, DNN and BiLSTM, are considered as a comparison. The dataset for training and test is generated through theoretical signal transduction analysis of the MTB communication system, and the BER performance of the proposed detectors is evaluated from various aspects. Taking the QS mechanism into account for receiver design, we consider two observed signals. One is the number of bacteria \mathbf{y}_N arriving at the receiver region, which is commonly taken as the receiver signal in MC works. The other is the luminescence intensity \mathbf{y}_L after QS process, which can be detected directly through photoelectric detection methods in our scenario. For observed signal \mathbf{y}_N with certain statistical information, the model-based optimal and sub-optimal MAP detectors are introduced as benchmarks. Results show that when there is a strong time-dependent relationship between consecutive symbols in the dataset due to ISI effect, the TCN and BiLSTM detectors can achieve better BER performance than sub-optimal MAP and DNN-based detectors, but behaves worse than optimal MAP detector. Moreover, if both the BER performance and complexity of the detectors are considered, the proposed TCN-based detector performs the best. In addition, for QS signal \mathbf{y}_L with an unknown underlying model, the proposed TCN-based detector

can basically achieve zero BER, whereas BiLSTM-based detector is slightly less stable and DNN-based detector has the worst performance. Also, if the QS signal y_L is accompanied with high AWGN, the proposed TCN-based detector shows the best BER performance, indicating that our proposed approach can achieve good robustness.

As part of future work, we plan to establish the experimental platform based on the proposed MTB communication system, through which the movement of information carriers can be precisely controlled by an external magnetic field, and the observed signal at the receiver can be detected conveniently. Furthermore, we would like to modify the structure and function of the information carriers to perform more complex tasks and to further improve the reliable transmission of MC system.

REFERENCES

- [1] N. Farsad, H. B. Yilmaz, A. Eckford, C.-B. Chae, and W. Guo, "A comprehensive survey of recent advancements in molecular communication," *IEEE Communications Surveys & Tutorials*, vol. 18, no. 3, pp. 1887–1919, Feb. 2016.
- [2] T. Nakano, M. J. Moore, F. Wei, A. V. Vasilakos, and J. Shuai, "Molecular communication and networking: Opportunities and challenges," *IEEE transactions on nanobioscience*, vol. 11, no. 2, pp. 135–148, May 2012.
- [3] V. Jamali, A. Ahmadzadeh, N. Farsad, and R. Schober, "Constant-composition codes for maximum likelihood detection without csi in diffusive molecular communications," *IEEE Transactions on Communications*, vol. 66, no. 5, pp. 1981–1995, Jan. 2018.
- [4] V. Jamali, A. Ahmadzadeh, C. Jardin, H. Sticht, and R. Schober, "Channel estimation for diffusive molecular communications," *IEEE Transactions on Communications*, vol. 64, no. 10, pp. 4238–4252, Aug. 2016.
- [5] N. Farsad and A. Goldsmith, "Neural network detection of data sequences in communication systems," *IEEE Transactions on Signal Processing*, vol. 66, no. 21, pp. 5663–5678, Sep. 2018.
- [6] O. D. Kose, M. C. Gursay, M. Saraclar, A. E. Pusane, and T. Tugcu, "Machine learning-based silent entity localization using molecular diffusion," *IEEE Communications Letters*, vol. PP, no. 99, pp. 1–1, Jan. 2020.
- [7] B.-H. Koo, H. J. Kim, J.-Y. Kwon, and C.-B. Chae, "Deep learning-based human implantable nano molecular communications," in *ICC 2020-2020 IEEE International Conference on Communications (ICC)*. IEEE, Jun. 2020, pp. 1–7.
- [8] Y. Huang, F. Ji, Z. Wei, M. Wen, and W. Guo, "Signal detection for molecular communication: model-based vs. data-driven methods," *IEEE Communications Magazine*, vol. 59, no. 5, pp. 47–53, May 2021.
- [9] H. B. Yilmaz, A. C. Heren, T. Tugcu, and C.-B. Chae, "Three-dimensional channel characteristics for molecular communications with an absorbing receiver," *IEEE Communications Letters*, vol. 18, no. 6, pp. 929–932, Apr. 2014.
- [10] L.-S. Meng, P.-C. Yeh, K.-C. Chen, and I. F. Akyildiz, "On receiver design for diffusion-based molecular communication," *IEEE Transactions on Signal Processing*, vol. 62, no. 22, pp. 6032–6044, Sep. 2014.
- [11] C. T. Chou, "A markovian approach to the optimal demodulation of diffusion-based molecular communication networks," *IEEE Transactions on Communications*, vol. 63, no. 10, pp. 3728–3743, Aug. 2015.
- [12] S. Kadloor, R. S. Adve, and A. W. Eckford, "Molecular communication using brownian motion with drift," *IEEE Transactions on NanoBioscience*, vol. 11, no. 2, pp. 89–99, Mar. 2012.
- [13] L. Lin, J. Zhang, M. Ma, and H. Yan, "Time synchronization for molecular communication with drift," *IEEE Communications Letters*, vol. 21, no. 3, pp. 476–479, Nov. 2016.
- [14] M. B. Miller and B. L. Bassler, "Quorum sensing in bacteria," *Annual Reviews in Microbiology*, vol. 55, no. 1, pp. 165–199, Oct. 2001.
- [15] A. Einolghozati, M. Sardari, and F. Fekri, "Design and analysis of wireless communication systems using diffusion-based molecular communication among bacteria," *IEEE transactions on wireless communications*, vol. 12, no. 12, pp. 6096–6105, Oct. 2013.
- [16] B. D. Unluturk, M. S. Islam, S. Balasubramaniam, and S. Ivanov, "Towards concurrent data transmission: Exploiting plasmid diversity by bacterial conjugation," *IEEE transactions on nanobioscience*, vol. 16, no. 4, pp. 287–298, May 2017.
- [17] B. Krishnaswamy, C. M. Henegar, J. P. Bardill, D. Russakow, G. L. Holst, B. K. Hammer, C. R. Forest, and R. Sivakumar, "When bacteria talk: Time elapse communication for super-slow networks," in *2013 IEEE International Conference on Communications (ICC)*. IEEE, Jun. 2013, pp. 6348–6353.
- [18] L. Grebenstein, J. Kirchner, W. Wicke, A. Ahmadzadeh, V. Jamali, G. Fischer, R. Weigel, A. Burkovski, and R. Schober, "A molecular communication testbed based on proton pumping bacteria: Methods and data," *IEEE Transactions on Molecular, Biological and Multi-Scale Communications*, vol. 5, no. 1, pp. 56–62, Oct. 2019.
- [19] W. Wicke, A. Ahmadzadeh, V. Jamali, H. Unterweger, C. Alexiou, and R. Schober, "Magnetic nanoparticle-based molecular communication in microfluidic environments," *IEEE transactions on nanobioscience*, vol. 18, no. 2, pp. 156–169, Jan. 2019.
- [20] S. Cho, T. C. Sykes, J. P. Coon, and A. A. Castrejón-Pita, "Electrophoretic molecular communication with time-varying electric fields," *Nano Communication Networks*, vol. 31, p. 100381, Mar. 2022.
- [21] S. Cho, J. P. Coon, T. C. Sykes, and A. A. Castrejón-Pita, "Intersymbol interference for electrophoretic molecular communication in circular duct channels," *IEEE Communications Letters*, vol. 26, no. 10, pp. 2307–2311, Oct. 2022.
- [22] Q. Wang and L. Zhang, "External power-driven microrobotic swarm: from fundamental understanding to imaging-guided delivery," *ACS nano*, vol. 15, no. 1, pp. 149–174, Jan. 2021.
- [23] T. Yin, Z. Diao, N. T. Blum, L. Qiu, A. Ma, and P. Huang, "Engineering bacteria and bionic bacterial derivatives with nanoparticles for cancer therapy," *Small*, vol. 18, no. 12, p. 2104643, Mar. 2022.
- [24] E. Steager, C.-B. Kim, J. Patel, S. Bith, C. Naik, L. Reber, and M. J. Kim, "Control of microfabricated structures powered by flagellated bacteria using phototaxis," *Applied Physics Letters*, vol. 90, no. 26, p. 263901, May 2007.
- [25] I. S. Khalil, M. P. Pichel, L. Abelmann, and S. Misra, "Closed-loop control of magnetotactic bacteria," *The International Journal of Robotics Research*, vol. 32, no. 6, pp. 637–649, Jun. 2013.
- [26] Q. Li, H. Chen, X. Feng, C. Yu, F. Feng, Y. Chai, P. Lu, T. Song, X. Wang, and L. Yao, "Nanoparticle-regulated semiartificial magnetotactic bacteria with tunable magnetic moment and magnetic sensitivity," *Small*, vol. 15, no. 15, p. 1900427, Mar. 2019.
- [27] L. Yang and L. Zhang, "Motion control in magnetic microrobotics: From individual and multiple robots to swarms," *Annual Review of Control, Robotics, and Autonomous Systems*, vol. 4, pp. 509–534, May 2021.
- [28] U. A. Chude-Onkonkwo, R. Malekian, B. T. Maharaj, and A. V. Vasilakos, "Molecular communication and nanonetwork for targeted drug delivery: A survey," *IEEE Communications Surveys & Tutorials*, vol. 19, no. 4, pp. 3046–3096, May 2017.
- [29] I. F. Akyildiz, M. Pierobon, S. Balasubramaniam, and Y. Koucheryav, "The internet of bio-nano things," *IEEE Communications Magazine*, vol. 53, no. 3, pp. 32–40, Mar. 2015.
- [30] M. M. Al-Zubi, A. S. Mohan, P. Plapper, and S. H. Ling, "Intrabody molecular communication via blood-tissue barrier for internet of bio-nano things," *IEEE Internet of Things Journal*, vol. 9, no. 21, pp. 21 802–21 810, Jun. 2022.
- [31] K. Aghababaiyan, H. Kebriaei, V. Shah-Mansouri, B. Maham, and D. Niyato, "Enhanced modulation for multiuser molecular communication in internet of nano things," *IEEE Internet of Things Journal*, vol. 9, no. 20, pp. 19 787–19 802, Apr. 2022.
- [32] S. Misra, S. Pal, and A. Mukherjee, "Bioblock: A blockchain analogous mechanism for integrity in iobnt-based drug delivery systems," *IEEE Systems Journal*, Aug. 2022.
- [33] L. Sun and Y. Wang, "Ctbrnn: A novel deep-learning based signal sequence detector for communications systems," *IEEE Signal Processing Letters*, vol. 27, pp. 21–25, Nov. 2019.
- [34] S. Bai, J. Z. Kolter, and V. Koltun, "An empirical evaluation of generic convolutional and recurrent networks for sequence modeling," *arXiv preprint arXiv:1803.01271*, Mar. 2018.
- [35] J. Müller, C. Kuttler, and B. A. Hense, "Sensitivity of the quorum sensing system is achieved by low pass filtering," *Biosystems*, vol. 92, no. 1, pp. 76–81, Apr. 2008.
- [36] J. J. Abbott, K. E. Peyer, M. C. Lagomarsino, L. Zhang, L. Dong, I. K. Kaliakatsos, and B. J. Nelson, "How should microrobots swim?" *The international journal of Robotics Research*, vol. 28, no. 11-12, pp. 1434–1447, Jul. 2009.

- [37] M. R. Bhatnagar *et al.*, "Characterization of bacteria signal propagation with an absorbing wall," *IEEE Communications Letters*, vol. 23, no. 4, pp. 744–747, Feb. 2019.
- [38] V. Jamali, A. Ahmadzadeh, W. Wicke, A. Noel, and R. Schober, "Channel modeling for diffusive molecular communication—a tutorial review," *Proceedings of the IEEE*, vol. 107, no. 7, pp. 1256–1301, Jun. 2019.
- [39] A. Noel, K. C. Cheung, and R. Schober, "Diffusive molecular communication with disruptive flows," in *2014 IEEE International Conference on Communications (ICC)*. IEEE, Jun. 2014, pp. 3600–3606.
- [40] R. V. Hogg, E. A. Tanis, and D. L. Zimmerman, *Probability and statistical inference*. Upper Saddle River, NJ, USA: Pearson/Prentice Hall, 2010.
- [41] G. Grimmett and D. Welsh, *Probability: an introduction*. London, U.K: Oxford University Press, 2014.
- [42] L. You, R. S. Cox, R. Weiss, and F. H. Arnold, "Programmed population control by cell–cell communication and regulated killing," *Nature*, vol. 428, no. 6985, pp. 868–871, Apr. 2004.
- [43] E. A. Meighen, "Genetics of bacterial bioluminescence," *Annual review of genetics*, vol. 28, no. 1, pp. 117–139, Dec. 1994.
- [44] R. Mosayebi, H. Arjmandi, A. Gohari, M. Nasiri-Kenari, and U. Mitra, "Receivers for diffusion-based molecular communication: Exploiting memory and sampling rate," *IEEE Journal on Selected Areas in Communications*, vol. 32, no. 12, pp. 2368–2380, Nov. 2014.
- [45] E. Dahlman, S. Parkvall, and J. Skold, *4G: LTE/LTE-advanced for mobile broadband*. Waltham, USA: Academic press, 2013.
- [46] H. Yao, D.-I. Zhu, B. Jiang, and P. Yu, "Negative log likelihood ratio loss for deep neural network classification," in *Proceedings of the Future Technologies Conference*. Springer, Oct. 2019, pp. 276–282.
- [47] J. H. Martin, *Speech and language processing: An introduction to natural language processing, computational linguistics, and speech recognition*. Upper Saddle River, NJ, USA: Pearson/Prentice Hall, 2009.
- [48] M. Schuster and K. K. Paliwal, "Bidirectional recurrent neural networks," *IEEE transactions on Signal Processing*, vol. 45, no. 11, pp. 2673–2681, Nov. 1997.
- [49] K. He, X. Zhang, S. Ren, and J. Sun, "Deep residual learning for image recognition," in *Proceedings of the IEEE conference on computer vision and pattern recognition*, Jun. 2016, pp. 770–778.
- [50] R. Nadkarni, S. Barkley, and C. Fradin, "A comparison of methods to measure the magnetic moment of magnetotactic bacteria through analysis of their trajectories in external magnetic fields," *PLoS one*, vol. 8, no. 12, p. e82064, Dec. 2013.
- [51] N. A. Licata, B. Mohari, C. Fuqua, and S. Setayeshgar, "Diffusion of bacterial cells in porous media," *Biophysical journal*, vol. 110, no. 1, pp. 247–257, Jan. 2016.